

Insight into particle retention and clogging in porous media; a pore scale study using lattice Boltzmann method

Amin Parvan^a, Saeed Jafari^{a,*}, Mohammad Rahnema^a, Saeid Norouzi apourvari^b, Amir Raoof^c

^a Department of Mechanical Engineering, Shahid Bahonar University of Kerman, Kerman, Iran

^b Department of Petroleum Engineering, Shahid Bahonar University of Kerman, Kerman, Iran

^c Department of Earth Sciences, Utrecht University, Utrecht, the Netherlands

ARTICLE INFO

Keywords:

Porous media
Clogging process
Lattice Boltzmann method
Porosity
Permeability reduction

ABSTRACT

Particle deposition in porous media alters hydraulic properties including porosity and permeability. The extent of these alterations depends on both porous media structure and its geometrical and topological properties. In the present study, a Lattice Boltzmann modeling is developed and used to systematically simulate particle clogging and to explore the evolution of hydraulic properties using realistic pore structures obtained from x-ray tomography.

A total of six different porous media are studied where three domains have different porosities and grain sizes, but the same pore connectivities, to explore the geometrical effects, and three domains have the same porosity but different grain arrangements and pore connectivities to study the effect of porous media topology. The results have shown the impact of the underlying pore-scale mechanisms resulting in porous media clogging and how they are affected by the initial porosity and topology of the media. Moreover, simulation has been utilized to develop porosity-permeability relations, covering the initial sample permeability all the way to complete clogging of the media where permeability vanishes. To provide more generic relations, the obtained coefficients of the porosity-permeability formulations are correlated to each porous media geometrical and topological properties.

1. Introduction

A wide range of environmental and engineering problems such as subsurface applications depend on transport of migrating solid particles and their deposition and clogging of the media (Vu et al., 2019; Kacimov and Obnosov, 2019). This includes treatment of septic tank effluent and wastewater (Jones and Taylor, 1965; Bouma, 1975; Beach and McCray, 2003; Abdoli et al., 2018a, 2018b), artificial recharges (Okubo and Matsumoto, 1983; Okubo and Matsumoto, 1979; Zhang et al., 2015), biological clogging in soil (Soleimani et al., 2009; Beniou et al., 2017), adsorption at fluid interfaces (Zhang et al., 2012, 2013), subsurface heat storage (Pfeiffer et al., 2000), spread of contaminant plumes and bioremediation (Molz et al., 1986; Baveye and Valocchi, 1989; Vandevivere et al., 1995), geologic carbon sequestration (Raoof et al., 2012, 2013), extraction of fossil energy, and in civil and environmental engineering applications. The blockage of porous media and permeability reduction of marine sediments caused by trapped fine particles is a common concern in application such as oil or natural gas extractions. In oilfields, to reduce the environmental damage and to increase the oil production the produced water is re-injected into the reser-

voir. The presence of solid particles in the injected water frequently causes an increase in injection pressure and therefore, a decrease in medium permeability. When pumping the groundwater, the retained particles accumulate near the well bore leading to the reduction or even total loss of the well capacity (de Zwart, 2007).

Estimating permeability value as a function of porosity, grain size, and the structure of fines in pore space can be challenging (A. Raoof et al., 2013). Porous media with a same porosity values often have different pore structures. This causes a non-unique relationship between porosity and permeability of porous media which is a reason for failure of models working based on first principles to predict clogging in porous media. Several different methods have been applied to study permeability reduction which includes experimental (Stephan and Chase, 2000; Mays and Hunt, 2005; Hubbe et al., 2009; Kim and Whittle, 2006) and numerical (Kampel et al., 2008; Raoof et al., 2013; Mahmoodlu et al., 2016; Ju et al., 2017) approaches. Most of the studies, however, are limited to domains with simple grain geometries such as cylindrical shapes. Hirabayashi et al. (2012) used Lattice Boltzmann Method (LBM) to study the motion and sedimentation of microscopic immersed particles in a viscous flow in a periodic porous media containing cylindrical grains. They found that particle trapping and

* Corresponding author.

E-mail address: jafari@uk.ac.ir (S. Jafari).

permeability reduction is mainly controlled by friction between particles and grain surfaces. Therefore, the surface roughness of particles and grains were the major clogging parameters. As the permeability alterations can be due to the attached particles as well as the moving ones with different velocities, they suggested that the ratio of the number of settled particles to the moving particles is a key parameter to characterize permeability reduction. [Sato et al. \(2013\)](#) used real sand grains and LBM to study the effect of trapped particles on reducing the permeability of porous media. They found that the reductions in permeability could not only be attributed to changes in volume fraction of the fine particles to the pore volume, but also to the size distribution of the fine particles. Their study showed that, when the porosity within the medium is roughly constant along the sample, whether the fine particles are fixed at random positions or are trapped at the narrow pore throats, the resulting permeabilities are of the same order of magnitude. They used volume fraction and the specific surface areas of both grains and clogging particles to define a relation for permeability alteration. To explore the accuracy of the applied numerical methods, [Qiu \(2015\)](#) studied the effect of different parameters including flow velocity and particle sizes in trapping of particles between grains using LBM and a hybrid Navier-Stokes method. They found that LBM is more accurate at close distances to the grain surfaces as it provides a better representation of the curved grain no-slip boundary conditions and the local velocity profile. In addition, there are a range of studies ([Pan et al., 2001](#); [Jin et al., 2004](#); [Boek and Venturoli, 2010](#)) that have utilized the LBM to simulate fluid flow and estimate permeability. [Ahfir et al. \(2016\)](#) investigated the influence of grain size distribution of the porous medium on clogging and found that the larger number of particles are deposited in the narrower pores. However, they did not state the fundamental mechanism of clogging in porous media caused by particle transport. [Boccardo et al. \(2014\)](#) applied clean bed Filtration Theory (CFT) for the simulation of experimental column tests at the pore scale. They investigated particle transport via Eulerian steady-state simulations, where particle concentration is solving by the corresponding advection–diffusion equation. They achieved an accurate and efficient integration of large nanoparticle transport into continuum models for lateral flow assays. [Khan et al. \(2017\)](#) used experimental observations to obtain permeability and porosity changes in porous media. They have combined discrete element method (DEM) and pore-scale network modeling and found that the dual pore-scale model can predict the permeability of the invaded core in the regions away from the injection face. They could predict the porosity by adding the effect of external filter cake. Based on their observation, while retention of large particles enhances the surface deposition of small particles, retention of small particles does not change the rate of entrapment for other small particle. [Anbar et al. \(2018\)](#) studied changes in permeability and Darcy coefficient due to compaction and sedimentation of sand migration for sphere packing by using of LBM. In their work, compaction effects were simulated by growth grain diameter in their media. Furthermore, they studied the effect of sedimentation of particles in porous media on permeability. It was found that permeability variation was directional where permeability change along the flow direction was almost twice of the other directions.

Clogging is known to depend on physical factors, which control hydrodynamic effects. Porosity is a geometrical property which determines the total pore space available for fluid flow and pore connectivity determines the topology of the media which controls the effectiveness of porosity to guide flow through the medium ([Raoof et al., 2013](#)). Several classical mathematical models consider particle transport without including the effect of clogging caused by sedimentation of particles. This consideration prevents local flow disturbances due to particle attachment and movements which may control the development of transport and clogging in the media. In this study, a two-way coupling considers the effect clogging on local fluid flow as well as the effect of fluid flow on the particle motion. We should note that the coupling does not involve the effect of particle motion on flow field, and it con-

siders the effect of particles on fluid flow once sedimentation is taken place.

Ideally, clogging can be investigated by considering the retention of colloids with real shapes and volume immersed in the fluid phases on the surface of grains. In this study, a total of six domains are used for pore scale simulation of clogging. Three real geometries, which have identical topologies but different porosities, are used to study porous media geometrical effects, and, the other three domains, where position of solid grains were changed, are used to study porous media topological effects. Two common relations linking permeability and porosity, i.e., Carman-Kozeny and Power law relations, were fitted to the results of Lattice Boltzmann modeling of all six domains to find the values of their coefficients and to further explore how these coefficients are related to porous media properties.

2. Methodology

The applied method in this study includes two steps for simulating the motion of microscopic solid particles in porous media: i) Simulating flow in porous media, and ii) Simulating particle transport. Lattice Boltzmann Method (LBM) provides convenient way to implement the boundary conditions compared to the other numerical methods. Therefore, LBM is suitable for simulating viscose flow in complex porous media geometries ([Liu et al., 2016](#); [Bakhshian et al. 2016](#); [Chen and Doolen, 1998](#); [Inamuro et al., 1999](#); [Bakhshian et al., 2019](#)).

We consider the following simplifying assumptions to simulate particle transport and sedimentation in porous media in response to fluid drag:

- The concentration of the point particles in the fluid is sufficiently low so that the moving particles in the flow do not affect the physical properties of fluid such as its dynamic viscosity and density. Therefore, these properties are considered constant through the simulations.
- Transport of particles is due to the hydrodynamic drag forces (i.e., the interaction between particles, gravity, van der Waals force and electrostatic double layer forces are not considered). This is often applied in studies where flow is horizontal ([Feng et al., 2015](#); [Jafari et al., 2010](#)).
- The criterion for sedimentation is the distance between the particle surface and the boundary of solid grains (i.e., it is assumed that the interaction forces are favorable and do not hinder attachment of particles after the come very close to the grain surfaces).

3. Mathematical modeling

3.1. Fluid flow simulation

Mass balance and momentum conservation equations for the flow of an incompressible Newtonian fluid, are described as:

$$\nabla \cdot \mathbf{u} = 0 \quad (1)$$

$$\rho \left(\frac{\partial \mathbf{u}}{\partial t} + \mathbf{u} \cdot \nabla \mathbf{u} \right) = -\nabla p + \mu \nabla^2 \mathbf{u} \quad (2)$$

where ρ , \mathbf{u} , p and μ are fluid density, vector velocity, pressure and fluid kinematic viscosity, respectively. Eqs. (1) and (2) are solved by using a two-dimensional lattice with 9 velocity vectors (D2Q9 model) via LBM with a single relaxation time (SRT) and a BGK (Bhatnagar–Gross–Krook) collision operator. Non-slip boundary condition is applied by using of bounce back boundary condition at the interface of fluid and solid grains. At each time step, LBM equations are solved in a transient form until steady-state flow is reached.

3.1.1. Overview of lattice Boltzmann method

The evolution of the fluid velocity field is modeled by the Lattice Boltzmann Equation with source term and BGK collision model of a density distribution function, given as:

$$f_{\alpha}(x + c_{\alpha}\Delta t, t + \Delta t) - f_{\alpha}(x, t) = -\frac{f_{\alpha}(x, t) - f_{\alpha}^{eq}(x, t)}{\tau} + \Delta t F_{\alpha} \quad (3)$$

here, f_{α} is distribution function for fluid flow and f_{α}^{eq} is the equilibrium distribution function used for direction “ α ”. In addition, “ c_{α} ”, “ τ ” and F_{α} mention velocity vector, hydrodynamic relaxation time and the component of external force in α -direction, respectively. The value of external force in our simulations in all directions is zero and other parameters are defined as:

$$f_{\alpha}^{eq} = \omega_{\alpha} \rho \left[1 + 3 \frac{c_{\alpha} \cdot \mathbf{u}}{C^2} + \frac{9}{2} \frac{(c_{\alpha} \cdot \mathbf{u})^2}{C^4} - \frac{3}{2} \frac{\mathbf{u} \cdot \mathbf{u}}{C^2} \right] \quad (4)$$

where “ C ” is related to the lattice sound speed and “ ω_{α} ” is the weight coefficient for the α -direction, for D2Q9 discrete velocity model expressed as:

$$C = \Delta x / \Delta t \quad (5)$$

$$Cs = C / \sqrt{3} \quad (6)$$

where Δx , Δt and Cs are lattice length and time step that both are selected as 1 and sound speed, respectively. Kinematic viscosity “ ν ” and weighting factor “ ω_{α} ” in α -direction are expressed as:

$$\nu = (\tau - 0.5)C_s^2 \quad (7)$$

$$\omega_{\alpha} = \begin{cases} \frac{4}{9} & \alpha = 0 \\ \frac{1}{9} & \alpha = 1, 2, 3, 4 \\ \frac{1}{36} & \alpha = 5, 6, 7, 8 \end{cases} \quad (8)$$

The macro variables, such as density of the fluid “ $\rho(\mathbf{x}, t)$ ” and the macroscopic fluid velocity “ $\mathbf{u}(\mathbf{x}, t)$ ” can be calculated using:

$$\rho(\mathbf{x}, t) = \sum_{\alpha} f_{\alpha}(\mathbf{x}, t) \quad (9)$$

$$\rho(\mathbf{x}, t) \mathbf{u}(\mathbf{x}, t) = \sum_{\alpha} f_{\alpha}(\mathbf{x}, t) \mathbf{c}_{\alpha} \quad (10)$$

For the D2Q9 model is employed, nine directions are considered for velocity as:

$$\mathbf{c}_{\alpha} = \begin{cases} 0 & \alpha = 0 \\ (\cos[(\pi(\alpha-1)/2)], \sin[(\pi(\alpha-1)/2)])C & \alpha = 1, 2, 3, 4 \\ (\cos[(\pi(\alpha-4-1)/2)], \sin[(\pi(\alpha-4-1)/2)])\sqrt{2} & \alpha = 5, 6, 7, 8 \end{cases} \quad (11)$$

3.2. Particle transport

3.2.1. Introduction of effective forces

The motion of particles in the porous medium is affected by drag force and Brownian force in our simulations. Using Lagrangian particle tracking, solid particles are followed using the equations of motion as:

$$m \frac{d\mathbf{v}}{dt} = \mathbf{F}^{drag} + \mathbf{F}^B \quad (12)$$

where \mathbf{v} , \mathbf{F}^{drag} and \mathbf{F}^B are particle velocity, drag force and Brownian force, respectively. When the Re number of the domain is low and particle is not close to channel wall, a particle experiences Stokes drag force computed by:

$$\mathbf{F}^{drag} = 6\pi\mu a_c(\mathbf{u} - \mathbf{v}) \quad (13)$$

where μ , a_c , \mathbf{u} and \mathbf{v} are viscosity, particle radius, fluid velocity and particle velocity which are next replaced in Eq. (3). Additionally, Brownian

motion for particles suspended in a liquid or gas, caused by collisions with molecules of the surrounding medium affects particle transport, particularly for small particles. The effective force due to the Brownian motion can be expressed as:

$$\mathbf{F}^B = 6\pi\mu a_c \sqrt{\frac{2D_0}{dt}} f_g(\mathbf{x}) \quad (14)$$

where the diffusivity in bulk solution is $D_0 = \frac{k_B T}{6\pi\mu a_c}$, where k_B , T , and dt are Boltzmann constant, temperature and time step size, respectively. Gaussian distribution function “ $f_g(\mathbf{x})$ ” is a continuous function which approximates the exact binomial distribution of physical events, expressed as:

$$f_g(\mathbf{x}) = \frac{1}{\sqrt{2\pi\sigma^2}} e^{-\frac{(\mathbf{x}-a)^2}{2\sigma^2}} \quad (15), \text{ where “}a\text{” and “}\sigma\text{”, the mean and the standard deviation of Gaussian distribution function, are set to 0 and 1, respectively.}$$

3.2.2. Deposition mechanism

In each time step, the flow is computed, and, afterwards, particle transport is calculated to obtain the location of the particle (i.e., Eq. (12)). Colloids may attach at the solid surfaces of the grains during their movement and can ultimately result in clogging of the individual pores as well as the whole porous media. In this study, the distance between the surface of colloid and grain surface is utilized to determine particle deposition. When the minimum distance between the particle and grain surface is close to the particle radius ($R_p + \epsilon$, where ϵ is a small distance representing interaction due to the surfaces electric potentials), particle will attach to the grain surface, and, therefore, removed from the fluid phase. As progressively more particles attach to the grain, the pore shape changes. In our simulations, when the accumulated volume of attached particles in a cell occupies more than 90% of the cell volume the fluid cell is converted to a solid cell. Having pore sizes becoming smaller due to attachment, there will be more fluid shear force inserted on the attached particles causing them to move towards the nearby depression zones with less fluid flow. In this study, we consider this effect based on the study by Benioug et al. (2017). When a particle is subject to attachment, we explore the host LBM cell as well as the neighboring cells to explore the locations with the minimum drag force to be considered as the attachment location. We have performed several simulations and found that neighboring cells are most realistically defined as cells with a maximum distance of half a grain radius from the initial attachment location. The attachment term represents deposition of particles due to several underlying mechanisms including interception, deposition, ripening and favorable DLVO net forces. The DLVO theory includes two major components which add up to provide the total interaction force (Seetha et al., 2014). These components are van der Waals forces, based on the interparticle distances, and the electrostatic double layer forces, based on the charges of colloids and grain surfaces (Seetha et al., 2017a, 2017b). Under favorable condition, which is assumed in this study, as both double layer forces (between colloids and grain surfaces) and the van der Waals forces are attractive, no energy barrier is developed to inhibit colloid deposition at grain surfaces. These processes results in attachment of colloids that come in close contact with the solid phase. The ripening phenomenon is also included as the attached particles become solid cells (i.e., collectors) to which additional colloids attachment can occur. Considering only the attachment mechanism, provides the advantage that the observed impact of porous media complexities (i.e., its geometry and topology) on clogging is caused by only one factor (i.e., particle attachment) rather than multiple parameters such as coupled attachment and detachment and their non-linear interactions. The type of porous media, the flowing fluid properties, and colloid properties determine whether colloid attachment is the operating mechanisms (Won et al., 2019; Boccardo et al., 2014; Cai and Zhang, 2016; Su et al., 2019) or colloid detachment should be also considered (Klimenko et al., 2020; Benioug et al., 2017; Yang and Balhoff, 2017).

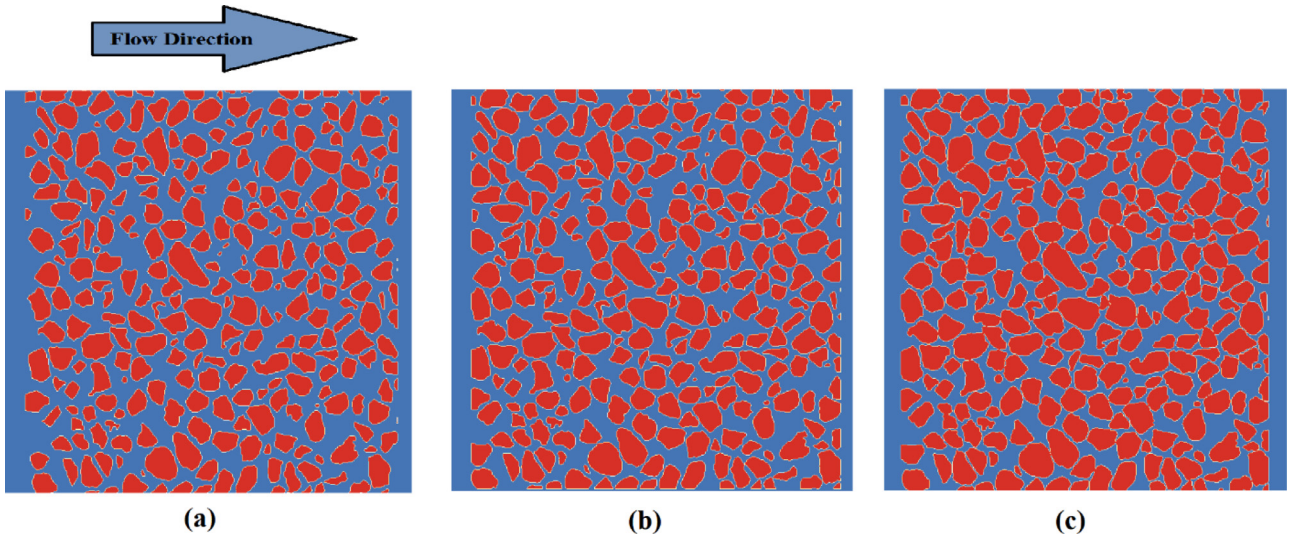


Fig. 1. Pore structures with different geometrical properties. The physical domain sizes were 800 micrometers in each direction. The size of the three pore-space domains is 800×800 micrometers with porosity of (a) $\phi_0 = 0.55$ (b) $\phi_0 = 0.50$ (c) $\phi_0 = 0.44$.

4. Results and discussion

We have considered a total of 6 different pore-scale domains to perform LBM simulations and colloid transport and clogging. The geometry of domains was obtained using x-ray tomography. To provide a set of three domains with similar topological properties (i.e., similar arrangement of pores and grains), but different porosity values (ϕ), we have numerically performed erosion on solid grains of the original domain, without changing grain locations, to obtain three domains with increasing porosity while keeping the pore connectivity unaffected (Fig. 1). This is done using ImageJ package (Rueden et al., 2017) where image pixels corresponding to the surface of the solid grains were removed in a layer-by-layer manner for all grains until a domain with a desired porosity value was obtained.

To explore the effect of different topologies under identical initial porosities, three extra pore structures were created. This is done by randomly swapping the location of individual solid grains as shown in Fig. 2.

For the simulations, the top and bottom flow boundaries were considered as no-flow and simulated by bounce back boundary condition. The inlet (located at the left side) and outlet (located at the right side) boundaries were considered as constant velocity and pressure, respectively. The half-way bounce back boundary condition was applied to the boundary of solid grains. The domain size and the particle diameter are 800×800 and 0.608 micrometers, respectively. After doing some grid independent tests, it was obvious that the best domain size is 500×500 in lattice unit. The ratio of solid density to fluid density and relaxation time (used in Eq. (7)) are taken as 1.05 and 0.65 in lattice unit, respectively. We have tested our model by simulating fluid flow in well-defined domain composed of cylindrical grains to obtain permeability and its corresponding Carman-Kozeny parameters for which verified data are available in the literature (Yazdchi et al., 2011). Colloids were injected through fluid flow with the constant flow velocity in inlet. Simulations show, initial distribution of particles in inlet has negligible effect on results (see appendix A). Colloids were injected at equal distances on a vertical cross section located behind the porous media inlet face.

4.1. Pore space evolution

The simulation results are used to compute the porosity and permeability values, and to investigate the relations between these two parameters. In each case, the simulation was continued until the complete clogging of the media is taken place as shown in Fig. 3. The obtained

two-dimensional distributions of the absorbed mass (shown by yellow color in Fig. 3) were used to calculate the profile of 1D averaged absorbed mass along the domain (Fig. 3b). To obtain the average values, the domain was divided into several sub-domains normal to the flow direction, and adsorbed mass was averaged in each sub-domain. Fig. 3b shows that a major part of clogging takes place at the inlet section of each domain, particularly for the domain with the initial porosity value of 0.44.

4.2. Porosity permeability relations for evolving porous media

We have chosen to fit the Carman-Kozeny and power law relations (Hommel et al., 2018) to our pore scale LBM simulations to obtain a relation between porosity and permeability. Moreover, these relations include coefficients which we have tried to relate them to the properties of each porous medium.

The measured porosity and permeability values for each sample are based on the whole domain size – rather than a subsection of the domain where, for example, most of clogging is taking place. This choice is based on the definition of Representative Elementary Volume (REV) requiring a domain of several pores/grains along each direction to provide representative macroscopic values. Given our initial domain sizes (with several pores along each principal direction), we have considered each whole domain as a REV and measured macroscopic properties and their evolutions by integrating within the whole domain. Doing so, our reported values, between different samples, are consistent with their initial porosity and permeability values, and also consistent with each other as they are all based on the whole domain size.

4.2.1. Carman-Kozeny and power-law relations

Carman-Kozeny (Kozeny, 1927; Carman, 1937; Hommel et al., 2018) is a well-known relation widely used to link porosity and permeability values in both experimental and modeling studies. This equation is based on simplifying porous media as parallel capillary tubes with equal geometry and size:

$$\frac{\Delta P}{L} = \frac{180\mu}{\phi_s^2 D_p^2} \frac{(1-\phi)^2}{\phi^3} v \quad (16)$$

where ϕ_s is sphericity, D_p and ϕ are particle diameter and porosity, respectively. This equation can be reformulated as:

$$K = \frac{\phi_s^2 D_p^2}{180} \frac{\phi^3}{(1-\phi)^2} \quad (17)$$

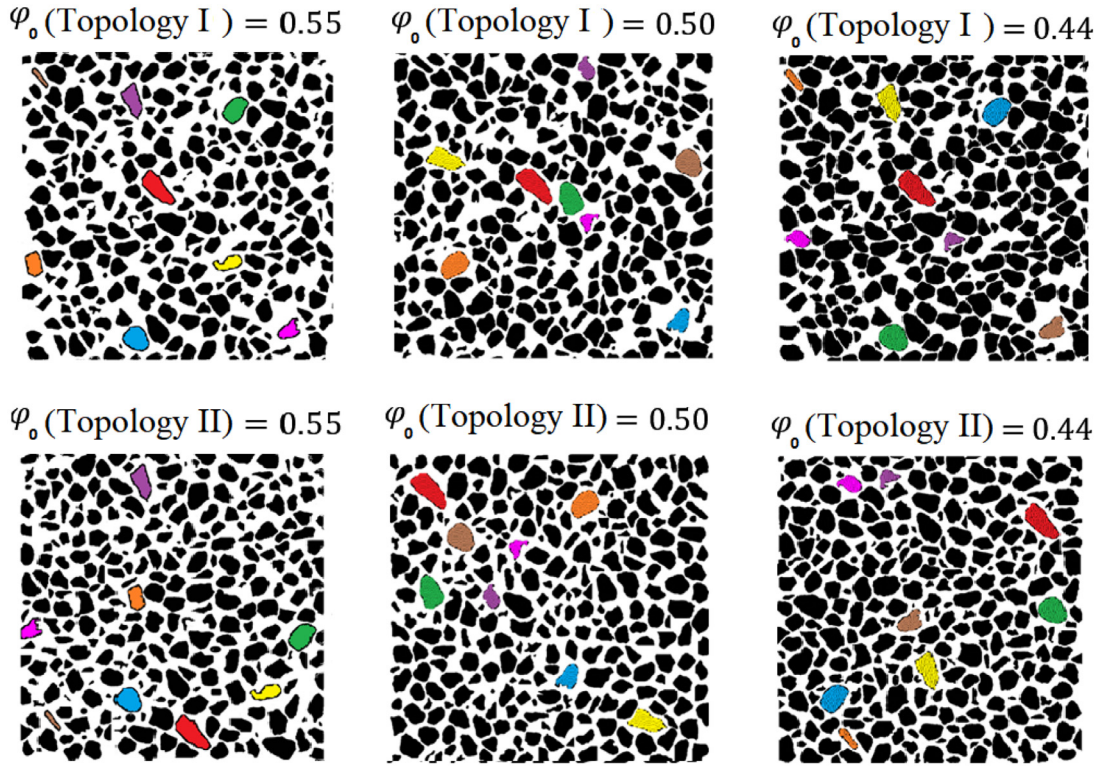


Fig. 2. Schematic of change in topology of porous media. Each column shows a pair with the same porosity, however, with different topology which is done randomly swapping the location of the solid grains. For the purpose of presentation, for each porosity (i.e., each column of the plot), a few of the swapped grains are colored to show the corresponding grain location changes between Topology I and II domains.

where K is permeability. Eq. (17) can be written as:

$$K = \frac{\varphi^3}{\sigma(1-\varphi)^2 s^2} \quad (18)$$

Eq. (18) is may be written using tortuosity, σ , and specific surface area, S , which compared to ϕ_s and D_p , are more relevant parameters to natural porous media (Gallo et al., 1998; MacQuarrie and Mayer, 2005). Mostaghimi et al. (2013) showed that using the Kozeny–Carman equation especially for complex, tortuous, heterogeneous, or poorly connected porous media significantly overestimates the permeability. The original Kozeny–Carman Equation may be also written as:

$$\frac{K}{K_0} = \frac{\varphi^3 S_0}{\varphi_0^3 S} \quad (19)$$

where, to provide a simpler formulation, the specific surface area, S , may be a replaced by $(1 - \varphi)$. During clogging, both porosity, φ , and specific surface area, S , change over time (S_0 is the initial specific surface area).

Due to clogging, permeability approaches zero without necessarily porosity approaching zero throughout the sample. To consider this effect, we applied a modified form of Carman-Kozeny relation as:

$$\frac{K}{K_0} = a \frac{\left(\frac{\varphi - \varphi_{cr}}{\varphi_0 - \varphi_{cr}} \right)^b}{\left(\frac{1 - \varphi + \varphi_{cr}}{1 - \varphi_0 + \varphi_{cr}} \right)^c} \quad (20)$$

where ϕ_0 , ϕ_{cr} and K_0 are the initial and critical porosity values and initial permeability, respectively. This equation is derived from Eqs. (17) and (18) and has been made dimensionless by using of K_0 , $(\phi_0 - \phi_{cr})$ and $(1 - \phi_0 + \phi_{cr})$ terms. The addition to this relation in comparison to the Eqs. (17) and (18) is the critical porosity, ϕ_{cr} , which is used to describe the nonzero porosity threshold at which the permeability approaches zero. The idea is that only for $\phi > \phi_{cr}$, the pore space is connected and thus only the pore space exceeding this limit

$(\phi - \phi_{cr})$ contributes to flow. Comparison the Eq. (20) with Eqs. (17) and (18) shows what values have been substituted with coefficients a , b and c .

In the original form of the Kozeny–Carman relation (provided in Section 4.2.1 Eq. (20); also studied by Wijngaarden et al., 2013; Steefel et al., 2015b; Xie et al., 2015; Pandey et al., 2015), changes in parameters related to geometry as sphericity, ϕ_s , or characteristic particle diameter, D_p , are assumed negligible. However, as geometry changes should be considered in our simulations, Eq. (20) was applied which has a similar form as the original Kozeny–Carman relation. Some studies (Marshall, 1958; Taylor et al., 1990) require calculations for geometrical corrections during damaging the pore structure. In our presented model, the only terms required to calculate are permeability and the starting and ending (critical) porosities.

Power law relation (Hommel et al., 2018; Verma and pruess, 1988; Ives and Pienvichitr, 1965) is another well-known relation widely used to describe permeability changes in both experimental and modeling studies. This provides a rather simple relation where the only major fitting parameter is the exponent “ b ”, and there is no strong term for specific changes of media geometry. This relation involves the medium specific exponent “ a ” as a parameter:

$$\frac{K}{K_0} = a \left(\frac{\varphi}{\varphi_0} \right)^b \quad (21)$$

In this study, the power-law relation is expresses as:

$$\frac{K}{K_0} = a \times \left(\frac{\varphi - \varphi_{cr}}{\varphi_0 - \varphi_{cr}} \right)^b \quad (22)$$

4.3. Fit on Carman-Kozeny and power-law relations

We have fitted the Carman-Kozeny and power-law relations to the computed porosity and permeability values obtained from LBM simula-

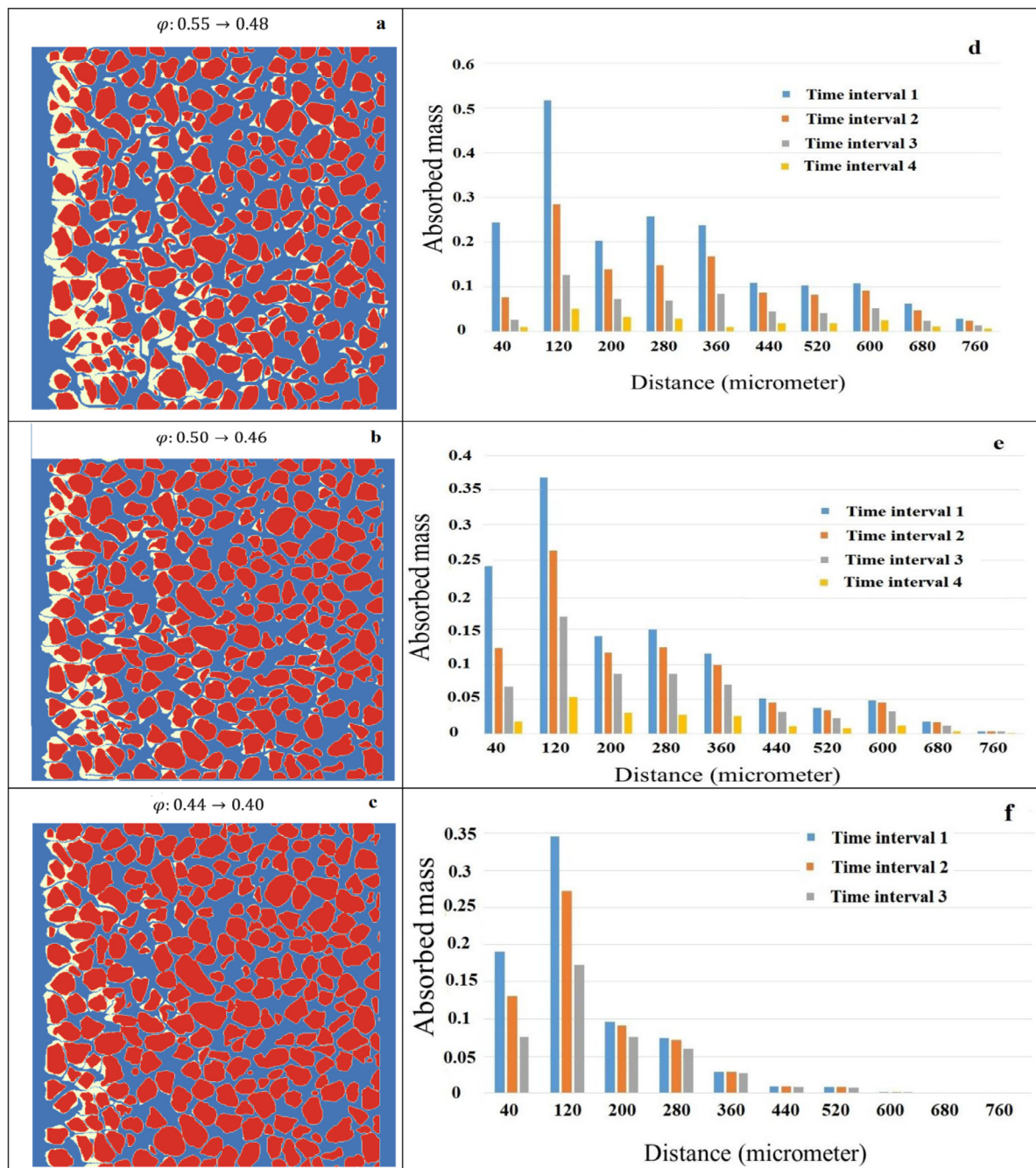


Fig. 3. The final pore space representing the clogged media with three different porosities (a, b and c). The yellow color shows the absorbed mass. Plots d, e and f show the cross-sectional-averaged absorbed mass (i.e., the 1D profile of the adsorbed mass along the overall flow direction) at different time moments chosen equally-spaced from each other and shown by blue, orange, gray, and brown colors, respectively. The plot orders correspond to domains a, b and c, respectively.

tions. Fig. 4 shows that porous media geometry and topology both influence the relation between permeability and porosity. Change of porous media topology affects the relation between permeability and porosity, and, moreover, changes the critical porosity of the media at which clogging takes place. This is specially the case for the media with the larger porosity of 55% as the presence of larger pores gives more freedom for particle movements by change of topology. Fig. 4 also shows a wide range of permeability for a given porosity value, which can vary even more than two folds. The solid lines in Fig. 4 are the plots of Carman-Kozeny and power-law relations (i.e., Eqs. (20) and (22)) describing the porosity-permeability relation based on the shown data points.

Table 1 provides properties of the porous media initially as well as after the clogging. All three cases have shown that the final porosities, under which permeability values tend to zero, are different for each topology.

Table 2 provides the coefficients of Carman-Kozeny relation. Coefficient “a” is nearly constant for both topologies and different initial porosities, coefficient “b” shows slightly more sensitivity to the initial porosity compared to the topology. Coefficient “c” shows dependency on both topology and initial porosity at low initial porosities and becomes less sensitive for domains with higher initial porosity. Comparing Eqs. (19) and (20) shows that coefficient “c” depends on specific

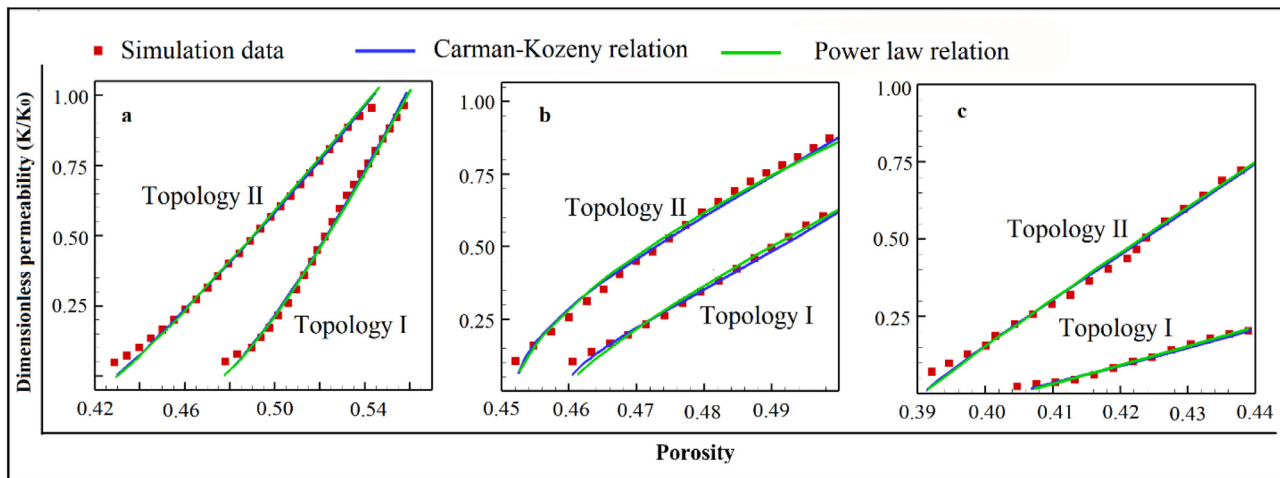


Fig. 4. Porosity-permeability relations where the square-shape data points indicate the result of LBM modeling and solid blue and green lines show the fitted Carman-Kozeny and power-law relations to the simulation results for different porous media porosities: a: $\phi_0 = 0.55$, b: $\phi_0 = 0.50$, c: $\phi_0 = 0.44$ and topologies. The parameter K_0 denotes initial/reference permeability of porous media, i.e., prior to retention of any particle at the boundary of solid grains. The value of the square of the correlation coefficient, R^2 , for all fittings were higher than 98%. Moreover, Appendix B provides simulation data and their fitted curves using a log scale plot.

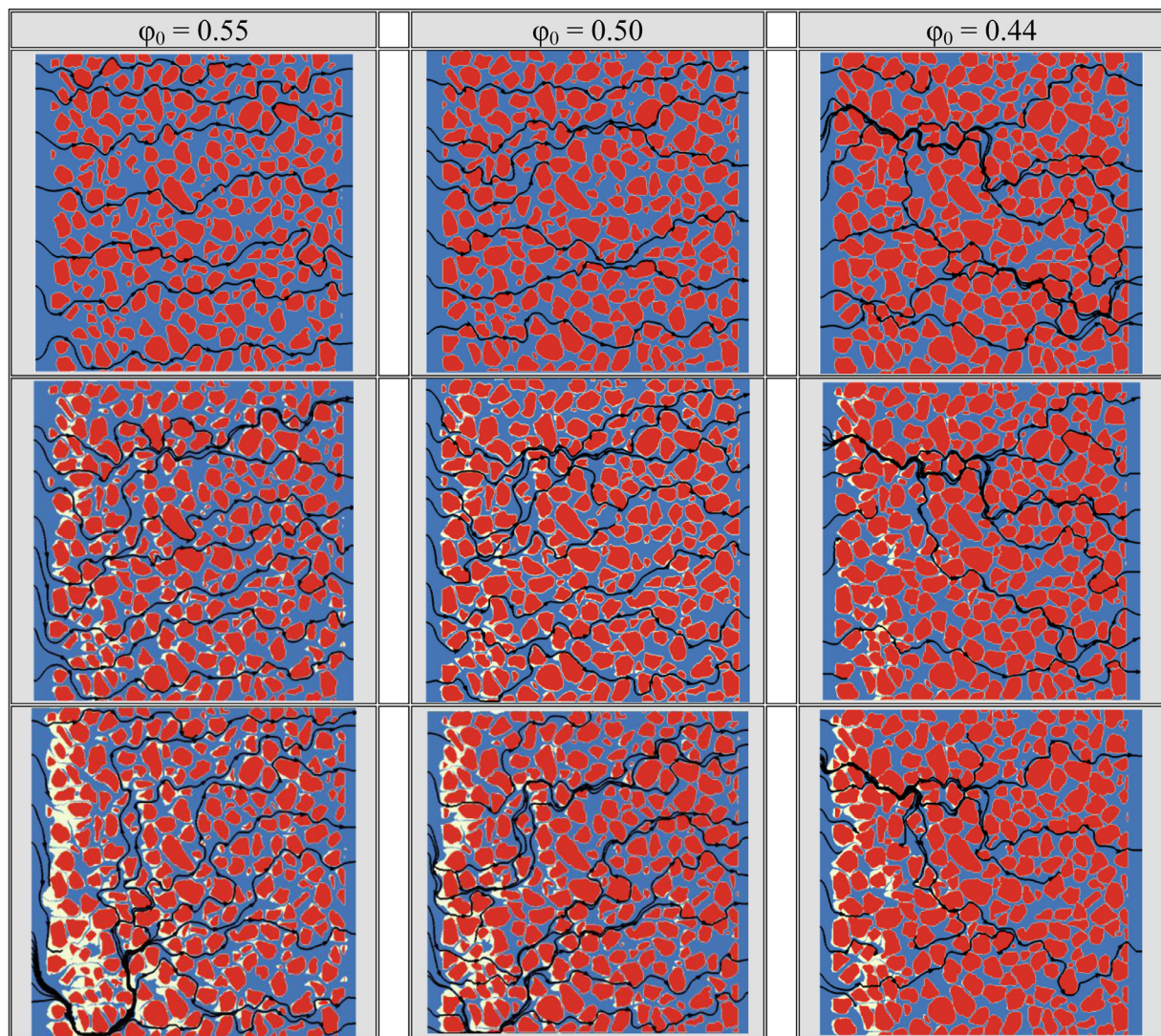


Fig. 5. Evolution of a set of streamlines, shown using black lines, over time as clogging proceeds for three domains with different geometries. Each column represents one domain geometry, with specific initial porosity, and shows clogging at over three consecutive times where the major streamlines become less in number and more tortuous.

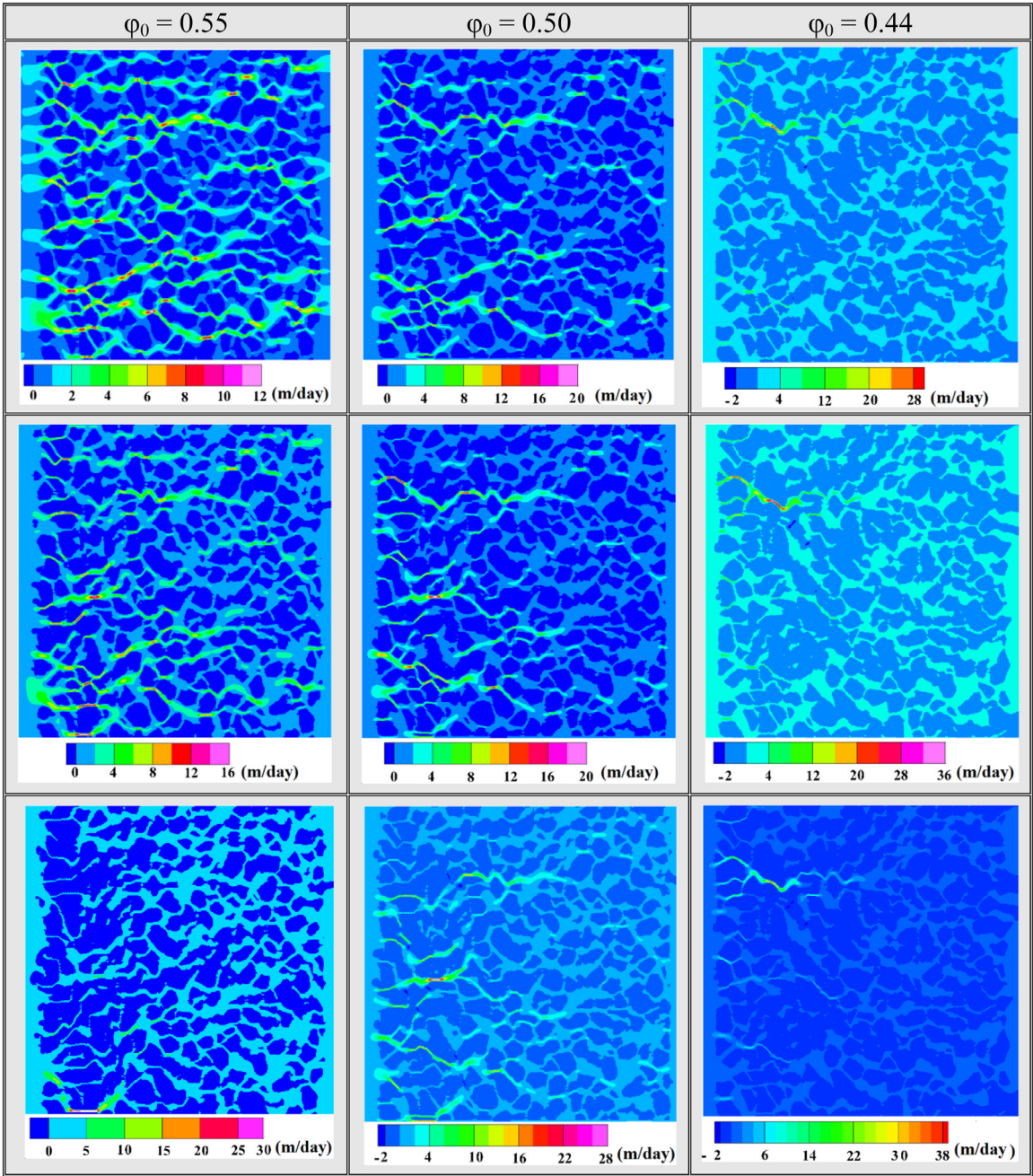


Fig. 6. Fluid velocity distributions for three geometries with different initial porosities over time during clogging (The unit of velocities is meters per day).

Table 1
Physical properties of the six domains with different geometries and topologies.

| | Topology | $\phi_0 = 0.55$ | $\phi_0 = 0.50$ | $\phi_0 = 0.44$ |
|---|----------|-----------------|-----------------|-----------------|
| Initial Average grain size(μm) | I, II | 35.95 | 37.90 | 40.46 |
| Final Average grain size(μm) | I, II | 39.56 | 40.14 | 41.68 |
| Final/critical Porosity (ϕ_{cr}) | I | 0.48 | 0.46 | 0.40 |
| | II | 0.43 | 0.45 | 0.39 |

Table 2
Coefficients of Carman-Kozeny relation (Eq. (20)) for six domains used in this study.

| Coefficient | Topology | $\phi_0 = 0.55$ | $\phi_0 = 0.50$ | $\phi_0 = 0.44$ |
|-------------|----------|-----------------|-----------------|-----------------|
| 'a' | I | 1.02 | 1.05 | 1.05 |
| | II | 1.05 | 1.08 | 1.05 |
| 'b' | I | 1.14 | 0.63 | 0.84 |
| | II | 1.11 | 0.46 | 0.79 |
| 'c' | I | 0.53 | 8.27 | 8.50 |
| | II | 0.68 | 7.43 | 4.66 |

surface area. As clogging affects the specific surface area and porosity of the media, coefficient “c” is sensitive to these two parameters. Schneider et al. (1996) used a form of Kozeny–Carman model that

the values of exponents “a” and “b” were set, respectively, to 3.0 and 2.0, and, in some cases, these values were changed depending on the rock type. Coefficient “c” in their model was assumed to be equal to

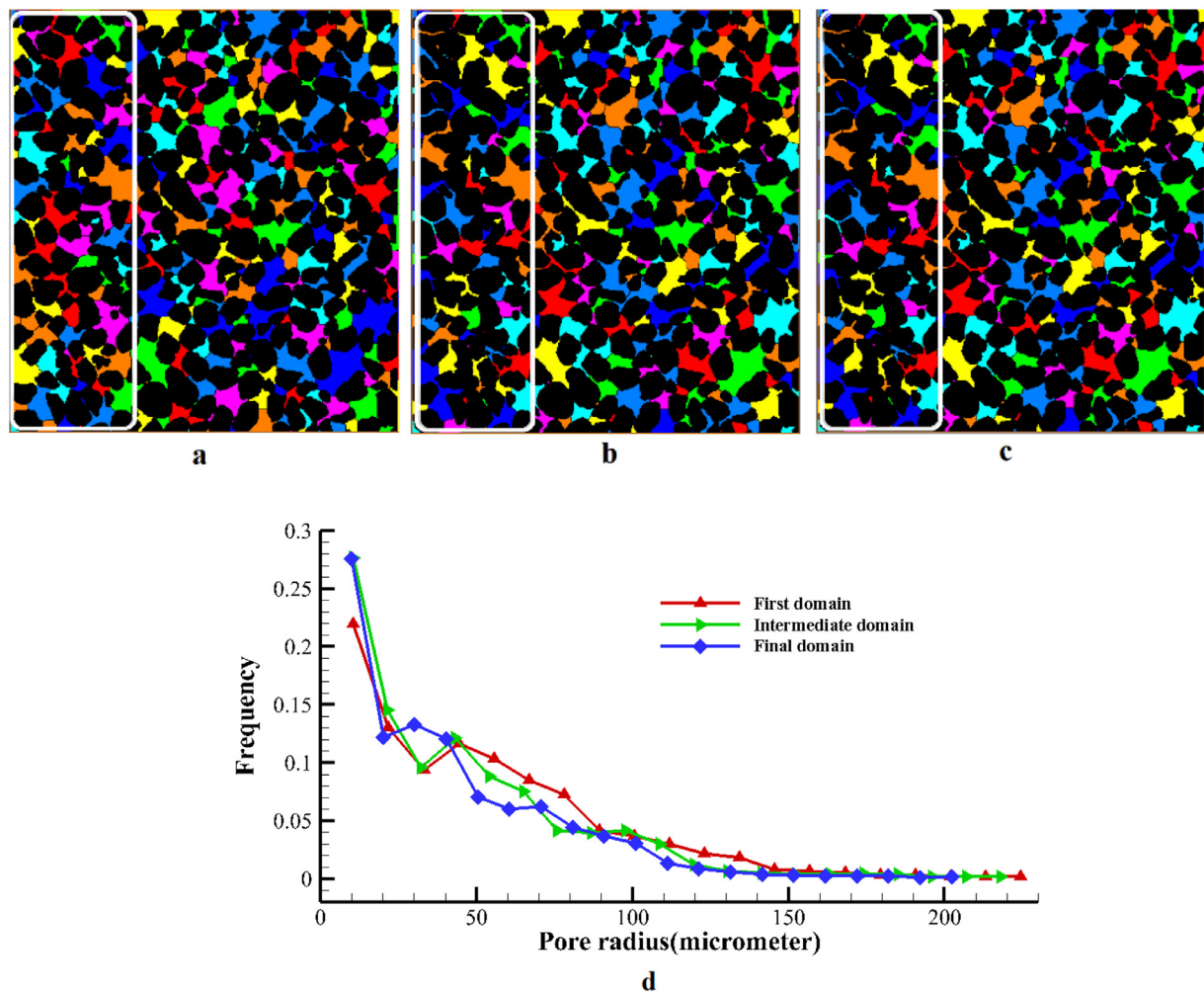


Fig. 7. The evolution of the pore space, where it becomes more disconnected over time, for the sample with the initial porosity of 0.55 (a, b and c) and the histograms showing change of pore sizes as clogging process (d).

Table 3
Coefficients of the power law relation in initial and changed geometry.

| Coefficient | Topology | $\phi_0 = 0.55$ | $\phi_0 = 0.50$ | $\phi_0 = 0.44$ |
|-------------|----------|-----------------|-----------------|-----------------|
| 'a' | I | 1.01 | 1.01 | 1.03 |
| | II | 1.02 | 1.03 | 1.03 |
| 'b' | I | 1.22 | 0.81 | 1.02 |
| | II | 1.08 | 0.63 | 0.95 |

1.0. Some studies (like Taylor et al., 1990; Vandevivere et al., 1995; Vandevivere et al., 1995; Martys et al., 1994) have replaced $(1 - \phi)$ term with the specific surface area, and considered the value of “a”, “b” and “c” to be equal to 3.0, 1.0 and 1.0, respectively. Using a rearranged form of Carman-Kozeny relation, Amaefule et al. (1993) set coefficients “a” and “b” to 3.0 and 2.0 and coefficient “c” was expressed as $\gamma = 1/S\sqrt{2\sigma}$. Based on the relation of Amaefule et al. (1993) together with the experimental data, Civan (2000) used another form of Carman-Kozeny relation, $\sqrt{\frac{K}{\phi}} = \gamma(\frac{\phi}{1-\phi})^\beta$, to find values of γ (4.1 - 5.82) and β (2.96 - 3.89).

Table 3 provides coefficient values corresponding to the power-law relation. Coefficient “a” remains nearly unchanged, while coefficient “b” indicates a strong dependency on both initial porosity and topology. The exponent “b” is an empirical parameter in Eq. (22) (Hommel et al., 2018). As discussed in Section 4.2.1, the initial porous medium properties, and the conditions that cause the pore geometry to change, de-

termine the value of “b”. For instance, Bernabe et al. (2003) suggested that the value of “b” is between 2.5 and 3.0 for plastic compaction, 8.0 for mineral precipitation, $b \geq 10.0$ for chemical alteration, and $b \geq 20.0$ for mineral dissolution. Doyen (1988) measured an evolving pore space and calibrated a value of $b = 3.8$ for water containing CO_2 . Garing et al. (2015) observed an increase in permeability which was fitted using a power-law relation with an exponent “b” ranging between 4.87 and 23.72. Verma and Pruess (1988) stated that the value of “b” may range from 6.0 to less than 1.0 depending on the porous material type which for their study ranged from 1.98 to 0.73 based on experimental data collected from sandstone units. In our study, the simulations resulted in values of exponent “b” between 0.63 and 1.22.

4.4. Effect of clogging on flow field streamlines

Pore clogging alters pore structures, which, in turn, changes the flow field and the fluid streamlines. Fig. 5 shows the change in the path of a set of streamlines during clogging. Particle retention at pore throats changes the preferential flow and streamlines become longer and more tortuous. At the same time, the major streamlines become less in number since the remaining free paths that fluid can freely flow through them, become less frequent, as shown in Fig. 5.

The corresponding velocity distributions of plots in Fig. 5 are shown in Fig. 6. Flow velocities with larger magnitudes and variations become more dominant close to the inlet of the sample where clogging is effectively taking place. Because of the mass conservation law, as dur-

ing clogging process in all three cases the number of main paths are decreased the fluid velocity magnitude becomes larger over time. Because of lower initial porosity in case $\phi_0 = 0.44$, active pore throats are clogged sooner and average fluid velocity over time is higher compared to the other two cases.

4.5. Effect of clogging on pore size evolution

To explore the effect of clogging on pore size evolution, we have chosen the sample with the initial porosity of 0.55 to analyze change of pore sizes from the initial state (i.e., $\phi_0 = 0.55$) until complete clogging (Fig. 7). The location of pore throats (i.e., the narrowest constrictions between pores) is used to divide the total pore space into an ensemble of individual pores which are marked by different colors in Fig. 7. The solid rectangles show a section of the domain close to the inlet where most of the clogging takes place and finally becomes disconnected (Fig. 7-c) to diminish the permeability.

The resulting pore size distributions at three different times (i.e., times corresponding to the initial, intermediate, and the final clogging state of the sample) are provided in Fig. 7-d. The distribution of pore sizes during clogging shows that clogging did not significantly affect the pore size distributions, and only pores smaller than 150 μm show a slight change in their population density. This is because while pore clogging significantly affects permeability by locally disconnecting flow pathways, a major fraction of pores remains unclogged, and, therefore, pore size changes are less noticeable compared to the permeability changes.

5. Summary and conclusion

Porosity and permeability are the two major transport properties of porous media and relating permeability to porosity changes is the subject of several studies. This study explored porosity changes due to particle transport and clogging and how permeability is affected by this change.

The realistic pore space was obtained using x-ray computed tomography, and further used to create several extra pore structures by modifying grain sizes as well as grain locations and their arrangements. This provided a total of six domains to systematically study the effect of geometrical parameters (i.e., porosity change due to alteration of grain sizes) and topological parameters (i.e., pore connectivity changes due to alteration in grain arrangements) on porous media clogging.

For each domain, fluid flow was simulated using a Lattice Boltzmann method and Lagrangian approach was applied to simulate transport of particles. A new method, based on velocity variations at the grain surface, was implemented to obtain the ultimate location of particle deposition after particles come close to the grain surface. Particle transport and clogging was continued up to full clogging of the media where permeability approached zero at a critical porosity which was different for each domain.

The macroscopic, i.e., sample-scale, behavior was described using Carman-Kozeny and power law relations to relate permeability to porosity variations. The use of systematic domains with different geometrical and topological properties enabled us to link the coefficients in the Carman-Kozeny and power law relations to porous media properties. In Carman-Kozeny relation, coefficient “a” was nearly constant with a value of 1.05 for different initial porosities and different topologies, however coefficient “b” was affected by the initial porosity while change in topology had not significant effect on it. Coefficient “c” showed strong dependency on both topology and initial porosity at low initial porosi-

ties and the dependency on topology reduced for domains with higher initial porosity. In power law relations, coefficient “a” remains nearly constant for different domains, while coefficient “b” indicated a strong dependency on both initial porosity and topology.

The preferred particle deposition close to the inlet of the sample and along the flow paths of particles caused a non-uniform change of porosity along the sample depending on geometrical and topological properties of the media. Therefore, internal variations of different parameters were studied, including profile of absorbed mass in each domain during clogging process, change of pore sizes, and the main streamlines and their evolution during clogging. The evolution of pore sizes during the clogging showed that the collection of pores with an intermediate size (relative to the range of pore sizes present in porous media) were affected the most by clogging. The main flow streamlines were initially short and uniformly distributed along the domain. However, during clogging, streamlines decreased in number and became much longer in length which shows an increase of tortuosity in the presence of pore clogging.

In this study, we employed 2D domains to enable us to perform several simulations needed for a systematic study and to obtain the optimum location for particle deposition based on the velocity variations at the grain surfaces. While these simulations provided valuable insight into the role of geometrical and topological parameters in porosity-permeability relations, 3D simulations are required to provide more realistic values for correlation parameters based on pore connectivities in the three-dimensional space. Furthermore, in the developed method particles are point objects when they are being transported in fluid. However, we have developed and tested a method to determine the realistic location of the attached particles based on the velocity distribution at the grain surface. The assumption of point particles in our method (up to the point that they are attached), makes it suitable for small particles for which the particles do not significantly disturb the fluid flow during their transport, and their effect on fluid flow is considerable only after they are attached and changed the pore space, and, therefore, affecting fluid flow.

Author statements

The corresponding author of this manuscript, certify that the contributors’ and conflicts of interest statements included in this paper are correct and have been approved by all co-authors.

Declaration of Competing Interest

The authors have no conflict of interest to declare.

Acknowledgments

We note that there are no data sharing issues since all of the numerical information is provided in the figures produced by solving the equations in the paper. We thank the anonymous reviewers for their insightful comments and suggestions. We thank Enno de Vries for his help on generating the pore scale domains.

Supplementary materials

Supplementary material associated with this article can be found, in the online version, at doi:[10.1016/j.advwatres.2020.103530](https://doi.org/10.1016/j.advwatres.2020.103530).

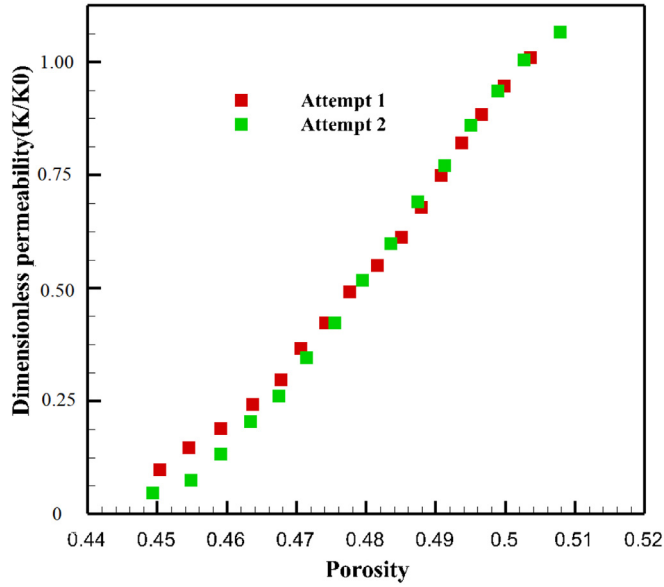


Fig. A1. Evaluation of sensitivity to the initial distributions of the particles at the inlet. In Attempt 1 particle were injected from cells with odd numbers, and, in Attempt 2, from every 5th cell along the inlet boundary.

Appendix

A: To evaluate the sensitivity of simulations to changes in the injection location of particles at the inlet, we performed simulations applying different initial distribution of particles at the inlet face of porous media. Fig. A1 shows that initial distribution of the particles has negligible effect on the relation between porosity and permeability. This can be explained as i) the domain is large enough and the inlet effects are not propagated through the whole media, and ii) the x-ray imaged pore structure used in this study is rather homogenous making it less sensitive to the conditions at the inlet.

B: Fig. A2, provides log scale plots for fitting of Carman-Kozeny and Power law relations (same data are shown using a linear scale in Fig. 4 of the manuscript). This figure shows that both relations were able to fit data and provided similar fit qualities.

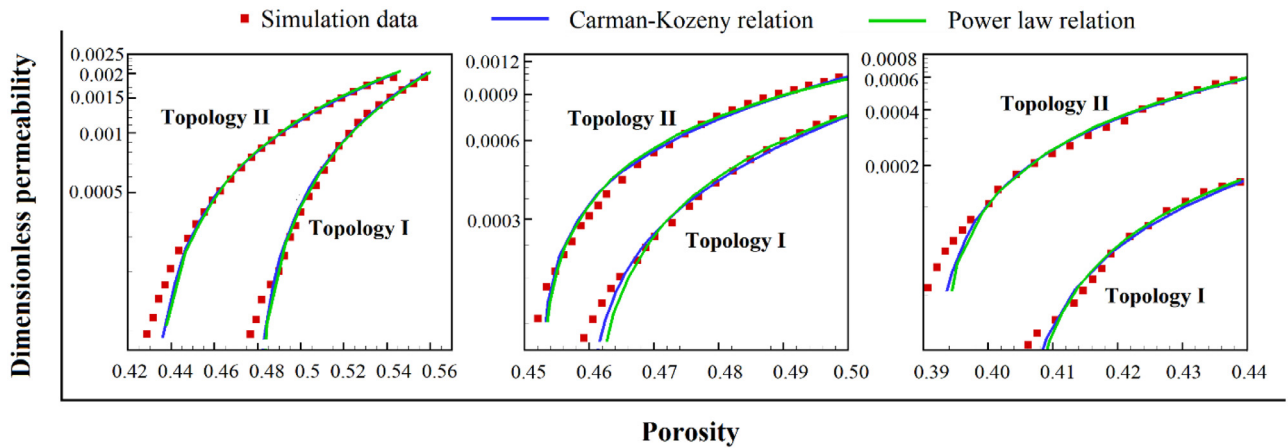


Fig. A2. Porosity-permeability relations shown in log scale where square symbols show data points from LBM modeling and the solid blue and green lines show the fitted Carman- Kozeny and power-law relations to the simulation results for different porous media with different porosities of a: $\phi_0 = 0.55$, b: $\phi_0 = 0.50$, c: $\phi_0 = 0.44$, as well as two different topologies. .

References

- Abdoli, S.M., Shafiei, S., Raoof, A., Ebadi, A., Jafarzadeh, Y., 2018a. Insight into heterogeneity effects in methane hydrate dissociation via pore-scale modeling. *Transp. Porous Media* 124 (1), 183–201.
- Abdoli, S.M., Shafiei, S., Raoof, A., Ebadi, A., Jafarzadeh, Y., Aslannejad, H., 2018b. Water flux reduction in microfiltration membranes: a pore network study. *Chem. Eng. Technol.* 41 (8), 1566–1576.
- Ahfir, N.D., Hammadi, A., Alem, A., Wang, H.Q., Le Bras, G., Ouahbi, T., 2016. Porous media grain size distribution and hydrodynamic forces effects on transport and deposition of suspended particles. *J. Environ. Sci.* <https://doi.org/10.1016/j.jes.2016.01.032>.
- Amaefule, J.O., Altunbay, M., Tiab, D., Kersey, D.G., Keelan, D.K., 1993. Enhanced reservoir description: using core and log data to identify hydraulic (flow) units and predict permeability in uncored intervals/wells. *Soc. Pet. Eng.* <https://doi.org/10.2118/26436-MS>.
- Anbar, S., Thompson, K.E., Tyagi, M., 2018. The impact of compaction and sand migration on permeability and non-darcy coefficient from pore-scale simulations. *Transp. Porous Media* <https://doi.org/10.1007/s11242-018-1190-3>.
- Bakhshian, S., Hosseini, S.A., Shokri, N., 2019. Pore-scale characteristics of multiphase flow in heterogeneous porous media using the lattice Boltzmann method. *Sci. Rep.* 9, 3377. <https://doi.org/10.1038/s41598-019-39741-x>.
- Bakhshian, S., Sahimi, M., 2016. Computer simulation of the effect of deformation on the morphology and flow properties of porous media. *Phys. Rev. E* 94 (4). <https://doi.org/10.1103/PhysRevE.94.042903>.
- Baveye, P., Valocchi, A., 1989. An evaluation of mathematical models of the transport of biologically reacting solutes in saturated soils and aquifers. *Water Resour. Res.* 25 (6), 1413–1421. <https://doi.org/10.1029/WR025i006p01413>.
- Beach, D., N.H. and McCray, J.E., 2009. Numerical modeling of unsaturated flow in wastewater soil absorption systems. *Groundwater Monitor. Remediat.* 23 (2), 64–72. <https://doi.org/10.1111/j.1745-6592.2003.tb00672.x>.
- Benioug, M., Golfier, F., Oltéan, C., Bués, M.A., Bahar, T., Cuny, T., 2017. An immersed boundary-lattice Boltzmann model for biofilm growth in porous media. *Adv. Water Resour.* 107, 65–82. <https://doi.org/10.1016/j.advwatres.2017.06.009>.
- Bernabe, Y., Mok, U., Evans, B., 2003. Permeability–porosity relationships in rocks subjected to various evolution processes. *Pure Appl. Geophys* 160 (5–6), 937960. <https://doi.org/10.1007/PL00012574>.
- Boccardo, G., Marchisio, D.L., Sethi, R., 2014. Microscale simulation of particle deposition in porous media. *J. Colloid Interface Sci.* 417, 227–237. <https://doi.org/10.1016/j.jcis.2013.11.007>.
- Boek, E.S., Venturoli, M., 2010. Lattice-Boltzmann studies of fluid flow in porous media with realistic rock geometries. *Comput. Math. Appl.* 59, 2305–2314. <https://doi.org/10.1016/j.camwa.2009.08.063>.
- Bouma, J., 1975. Unsaturated flow during soil treatment of septic tank effluent. *J. Environ. Eng. Div.* 101 (6), 967–983. <https://doi.org/10.1128/AEM.00560-08>.
- Cai, R., Zhang, L.-Z., 2016. Modeling of dynamic deposition and filtration processes of airborne particles by a single fiber with a coupled lattice Boltzmann and discrete element method. *Build. Environ.* <https://doi.org/10.1016/j.buildenv.2016.07.001>.
- Carman, P.C., 1937. Fluid flow through granular beds. *Trans. Inst. Chem. Eng.* 15, 150166.
- Chen, S., Doolen, G.D., 1998. Lattice Boltzmann method for fluid flows. *Annu. Rev. Fluid Mech.* 30, 329–364. <https://doi.org/10.1146/annurev.fluid.30.1.329>.
- Civan, F., 2000. Predictability of porosity and permeability alterations by geochemical and geomechanical rock and fluid interactions. *Soc. Pet. Eng.* <https://doi.org/10.2118/58746-MS>.
- De Zwart, A.H., 2007. Investigation of clogging processes in unconsolidated aquifers near water supply wells PhD Thesis. Tech. Univ. Delft, The Netherlands.
- Doyen, P.M., 1988. Permeability, conductivity, and pore geometry of sandstone. *J. Geophys. Res.* 93 (B7), 77297740. <https://doi.org/10.1029/JB093iB07p07729>, *Solid Earth*.
- Feng, Q., Li, S., Han, X., Wang, S., 2015. Network simulation for formation impairment due to suspended particles in injected water. *J. Petrol. Sci. Eng.* 133, 384–391. <https://doi.org/10.1016/j.petrol.2015.06.027>.
- Gallo, L.Y., Bildstein, O., Brosse, E., 1998. Coupled reaction-flow modeling of diagenetic changes in reservoir permeability, porosity and mineral compositions. *J. Hydrol.* 209, 366–388.
- Garing, C., Gouze, P., Kassab, M., Riva, M., Guadagnini, A., 2015. Anti-correlated porosity–permeability changes during the dissolution of carbonate rocks: experimental evidences and modeling. *Transp. Porous Media* 107 (2), 595–621. <https://doi.org/10.1007/s11242-015-0456-2>.
- Hirabayashi, S., Sato, T., Mitsuohori, K., Yamamoto, Y., 2012. Microscopic numerical simulations of suspension with particle accumulation in porous media. *Powder Technol.* 225, 143–148. <https://doi.org/10.1016/j.powtec.2012.04.001>.
- Hommel, J., Coltman, E., Class, H., 2018. Porosity–Permeability relations for evolving pore space: a review with a focus on (Bio-)geochemically altered porous media. *Transp. Porous Media* 124, 589–629. <https://doi.org/10.1007/s11242-018-1086-2>.
- Hubbe, M.A., Chen, H., Heitmann, J.A., 2009. Permeability reduction phenomena in packed beds, fiber mats, and webs of paper exposed to flow of liquids and suspensions: a review. *Bioresources* 4 (1), 405–451.
- Inamuro, T., Yoshino, M., Ogino, F., 1999. Lattice boltzmann simulation of flows in a three-dimensional porous structure. *Int. J. Numer. Methods Fluids* 29 (7), 737–748. [https://doi.org/10.1002/\(SICI\)1097-0363\(19990415\)29:7<737::AID-FLD813>3.0.CO;2-H](https://doi.org/10.1002/(SICI)1097-0363(19990415)29:7<737::AID-FLD813>3.0.CO;2-H).
- Ives, K., Pienvichitr, V., 1965. Kinetics of the filtration of dilute suspensions. *Chem. Eng. Sci.* 20 (11), 965973.
- Su, J., Chai, G., Wang, L., Cao, W., Gu, Z., Chen, C., Yun Xu, X., 2019. Pore-scale direct numerical simulation of particle transport in porous media. *Chem. Eng. Sci.* <https://doi.org/10.1016/j.ces.2019.01.033>.
- Jafari, S., Salmanzadeh, M., Rahnama, M., Ahmadi, G., 2010. Investigation of particle dispersion and deposition in a channel with a square cylinder obstruction using the lattice Boltzmann method. *J. Aerosol Sci.* 41 (2), 198–206. <https://doi.org/10.1016/j.jaerosci.2009.10.005>.
- Jin, S., Takeya, S., Hayashi, J., Nagao, J., Kamata, Y., Ebinuma, T., Narita, H., 2004. Structure analyses of artificial methane hydrate sediments by Microfocus X-ray computed tomography. *Jpn. J. Appl. Phys.* 43, 5673–5675. <https://doi.org/10.1143/JJAP.43.5673>.
- Jones, J.H., Taylor, G.S., 1965. Septic tank effluent percolation through sands under laboratory conditions. *Soil Sci.* 99 (5), 301–309.
- Ju, B., Yang, Y., Brantson, T., Chi, J., 2017. A numerical simulator developed for modeling permeability control for enhanced oil recovery. *J. Petrol. Sci. Eng.* <https://doi.org/10.1016/j.petrol.2017.08.056>.
- Kacimov, A.R., Obnosov, Y., 2019. Modelling of 2-D seepage from aquifer towards stream via clogged bed: the toth-treffitz legacy conjugated. *Adv. Water Resour.* 131, 103372. <https://doi.org/10.1016/j.advwatres.2019.07.002>.
- Kampel, G., Goldsztein, G.H., Santamarina, C., 2008. Plugging of porous media and filters: maximum clogged porosity. *Appl. Phys. Lett.* 92, 084101. <https://doi.org/10.1063/1.2883947>.
- Khan, H.J., Mirabolghasemi, M.S., Yang, J., Prodanovic, M., DiCarlo, D.A., Balhoff, M.T., 2017. Study of formation damage caused by retention of bi-dispersed particles using combined pore-scale simulations and particle flooding experiments. *J. Petrol. Sci. Eng.* 158, 293–308. <https://doi.org/10.1016/j.petrol.2017.08.061>.
- Kim, Y.S., Whittle, A.J., 2006. Filtration in a porous granular medium: 1. Simulation of pore scale particle deposition and logging. *Transp. Porous Media* 65, 53–87. <https://doi.org/10.1007/s11242-005-6087-2>.
- Kozeny, J., 1927. Über kapillare Leitung des Wassers im Boden. *Sitzungsber Akad Wiss Wien* 136 (2a), 271306.
- Liu, H., Kang, Q., Leonardi, C., Schmieschek, S., Narváez, A., Jones, B., Williams, J., Valocchi, A., Harting, J., 2016. Multiphase lattice Boltzmann simulations for porous media applications. *Comput. Geosci.* 20 (4), 777–805. <https://doi.org/10.1007/s10596-015-9542-3>, August 2016.
- Klimenko, Lyudmila S., Maryshev, Boris S., 2020. Numerical simulation of microchannel blockage by the random walk method. *Chem. Eng. J.* 381, 122644. <https://doi.org/10.1016/j.cej.2019.122644>.
- MacQuarrie, K.T.B., Mayer, K.U., 2005. Reactive transport modeling in fractured rock: A state-of-the-science review. *Earth-Sci. Rev.* 72, 189–227.
- Mahmoodlu, M.G., Raoof, A., Sweijen, T., Van Genuchten, M.T., 2016. Effects of sand compaction and mixing on pore structure and the unsaturated soil hydraulic properties. *Vadose Zone J.* 15 (8).
- Marshall, T.J., 1958. A relation between permeability and size distribution of pores. *J. Soil Sci.* 9 (1), 18. <https://doi.org/10.1111/j.1365-2389.1958.tb01892.x>.
- Martys, N.S., Torquato, S., Bentz, D.P., 1994. Universal scaling of fluid permeability for sphere packings. *Phys. Rev. E* 50, 403–408. <https://doi.org/10.1103/PhysRevE.50.403>.
- Mays, D.C., Hunt, J.R., 2005. Hydrodynamic aspects of particle clogging in porous media. *Environ. Sci. Technol.* 39, 577–584.
- Molz, F.J., Widdowson, M.A., Benefield, L.D., 1986. Simulation of microbial growth dynamics coupled to nutrient and oxygen transport in porous media. *Water Resour. Res.* 22 (8). <https://doi.org/10.1029/WR022i008p01207>, August 1986.
- Okubo, T., Matsumoto, J., 1979b. Effect of infiltration rate on biological clogging and water quality changes during artificial recharge. *Water Resour. Res.* 15 (6), 1536–1542. <https://doi.org/10.1029/WR015i006p01536>.
- Okubo, T., Matsumoto, J., 1979a. Biological clogging of sand and changes of organic constituents during artificial recharge. *Water Res.* 17 (7), 813–821. [https://doi.org/10.1016/0043-1354\(83\)90077-5](https://doi.org/10.1016/0043-1354(83)90077-5).
- Pan, C., Hilpert, M., Miller, C.T., 2001. Pore-scale modeling of saturated permeabilities in random sphere packing. *Phys. Rev. E* 64. <https://doi.org/10.1103/PhysRevE.64.066702>, 066702-1-9.
- Pandey, S., Chaudhuri, A., Rajaram, H., Kelkar, S., 2015. Fracture transmissivity evolution due to silica dissolution/precipitation during geothermal heat extraction. *Geothermics* 57, 111–126. <https://doi.org/10.1016/j.geothermics.2015.06.011>.
- Pfeiffer, S.R., Ragusa, S., Sztajnbock, S., Vandeveld, T., 2000. Interrelationships between biological, chemical, and physical processes as an analog to clogging in aquifer storage and recovery (ASR) wells. *Water Res.* 34 (7), 2110–2118. [https://doi.org/10.1016/S0043-1354\(99\)00356-5](https://doi.org/10.1016/S0043-1354(99)00356-5).
- Qiu, Q., 2015. Theoretical and computational study of colloid transport and retention in saturated soil porous media. Univer. Delaware (PhD thesis). Citable URI <http://udspace.udel.edu/handle/19716/17595>.
- Raoof, A., Nick, H.M., SM Hassanizadeh, H.M., Spiers, C.J., 2013. PoreFlow: a complex pore-network model for simulation of reactive transport in variably saturated porous media. *Comput. Geosci.* 61, 160–174.
- Raoof, A., Nick, H.M., Wolterbeek, T.K.T., Spiers, C.J., 2012. Pore-scale modeling of reactive transport in wellbore cement under CO2 storage conditions. *Int. J. Greenhouse Gas Control* 11, S67–S77.
- Rueden, C.T., Schindelin, J., Hiner, M.C., et al., 2017. "ImageJ2: imageJ for the next generation of scientific image data. *BMC Bioinform.* 18, 529. <https://doi.org/10.1186/s12859-017-1934-z>, PMID 29187165.
- Sato, T., Mitsuohori, K., Hirabayashi, S., Brumby, P.E., Nagao, J., Temma, N., Narita, H., 2013. Micro scale 551 numerical simulation of the permeability reduction due to trapping of suspended fine particles 552 within sand sediments. *Transp. Porous Media* 96 (1), 153–167. <https://doi.org/10.1007/s11242-012-0079-9>.
- Seetha, N., Hassanizadeh, S.M., Kumar, M.S.M., Raoof, A., 2017a. Correlation equations for average deposition rate coefficients of nanoparticles in a cylindrical pore. *Water Resour. Res.* 51 (10), 8034–8059.
- Seetha, N., Kumar, M.S.M., Hassanizadeh, S.M., Raoof, A., 2014. Virus-sized colloid trans-

- port in a single pore: model development and sensitivity analysis. *J. Contam. Hydrol.* 164, 163–180.
- Seetha, N., Raoof, A., Kumar, M.S.M., Hassanizadeh, S.M., 2017b. Upscaling of nanoparticle transport in porous media under unfavorable conditions: pore scale to Darcy scale. *J. Contam. Hydrol.* 200, 1–14.
- Schneider, F., Potdevin, J., Wolf, S., Faille, I., 1996. Mechanical and chemical compaction model for sedimentary basin simulators. *Tectonophysics* 263 (1), 307–317. [https://doi.org/10.1016/S0040-1951\(96\)00027-3](https://doi.org/10.1016/S0040-1951(96)00027-3).
- Soleimani, M., Hosseini, S., Roostaazad, R., Petersen, J., Mousavi, S.M., Vasiri, A.K., 2009. Microbial leaching of a low-grade sphalerite ore using a draft tube fluidized bed bioreactor. *Hydrometallurgy* 99, 3–4. 131–136 <http://hdl.handle.net/11427/21249>.
- Steeffel, C.I., Yabusaki, S.B., Mayer, K.U., 2015b. Reactive transport benchmarks for subsurface environmental simulation. *Comput. Geosci.* 19 (3), 439443. <https://doi.org/10.1007/s10596-015-9499-2>.
- Stephan, E.A., Chase, G.G., 2000. Development of volume-average theory for deep-bed filtration. *AIChE J.* 46 (10), 1918–1926. <https://doi.org/10.1002/aic.690461004>.
- Taylor, S.W., Milly, P.C.D., Jaff, P.R., 1990. Biofilm growth and the related changes in the physical properties of a porous medium: 2. Permeability. *Water Resour. Res.* 26 (9), 2161–2169. <https://doi.org/10.1029/WR026i009p02161>.
- Van Wijngaarden, W.K., Vermolen, F.J., Meurs, G.A.M., Vuik, C., 2013. A mathematical model for Biogrout. *Comput. Geosci.* 17 (3), 463478. <https://doi.org/10.1007/s10596-012-9316-0>.
- Vandevivere, P., Baveye, P., de Lozada, D.S., DeLeo, P., 1995. Microbial clogging of saturated soils and aquifer materials: evaluation of mathematical models. *Water Resour. Res.* 31 (9), 2173–2180. <https://doi.org/10.1029/95wr01568>.
- Verma, A., Pruess, K., 1988. Thermohydrological conditions and silica redistribution near high-level nuclear wastes emplaced in saturated geological formations. *J. Geophys. Res.: Solid Earth* 93 (B2), 11591–11593. <https://doi.org/10.1029/JB093iB02p01159>.
- Vu, M.T., Jardani, A., Krimissa, M., Fischer, P., Ahfir, N., 2019. Hydraulic tomography in time-lapse mode for tracking the clogging effects associated with the colloid injection. *Adv. Water Resour.* 133, 103424. <https://doi.org/10.1016/j.advwatres.2019.103424>.
- Won, J., Lee, D., Pham, K., Lee, H., Choi, H., 2019. Impact of particle size distribution of colloidal particles on contaminant transport in porous media. *Appl. Sci.* 9 (5), 932. <https://doi.org/10.3390/app9050932>.
- Xie, M., Mayer, K.U., Claret, F., Alt-Epping, P., Jacques, D., Steefel, C., Chiaberge, C., Simunek, J., 2015. Implementation and evaluation of permeability-porosity and tortuosity-porosity relationships linked to mineral dissolution-precipitation. *Comput. Geosci.* 19 (3), 655671. <https://doi.org/10.1007/s10596-014>.
- Yang, H., Balhoff, M.T., 2017. Pore-network modeling of particle retention in porous media. *AIChE J.* 63, 3118–3131. <https://doi.org/10.1002/aic.15593>.
- Yazdchi, K., Srivastava, S., Luding, S., 2011. Microstructural effects on the permeability of periodic fibrous porous media. *Int. J. Multiphase Flow* 37 (8), 956–966. <https://doi.org/10.1016/j.ijmultiphaseflow.2011.05.003>.
- Zhang, Q., Hassanizadeh, S.M., Karadimitriou, N.K., Raoof, A., Liu, B., 2013. Retention and remobilization of colloids during steady-state and transient two-phase flow. *Water Resour. Res.* 49 (12), 8005–8016.
- Zhang, Q., Hassanizadeh, S.M., Raoof, A., van Genuchten, M.T., Roels, S.M., 2012. Modeling virus transport and remobilization during transient partially saturated flow. *Vadose Zone J.* 11 (2).
- Zhang, Q., Raoof, A., Hassanizadeh, S.M., 2015. Pore-scale study of flow rate on colloid attachment and remobilization in a saturated micromodel. *J. Environ. Qual.* 44 (5), 1376–1383.